Partitioning of interaction energy in van der Waals complexes involving excited state species: The $He(^1S)+Cl_2(B\,^3\Pi_u)$ interaction

Sl/awomir M. CybulskiRudolf BurclGrzegorz Chal/asińskiM. M. Szczęśniak

Citation: The Journal of Chemical Physics **103**, 10116 (1995); doi: 10.1063/1.469913
View online: http://dx.doi.org/10.1063/1.469913
View Table of Contents: http://aip.scitation.org/toc/jcp/103/23
Published by the American Institute of Physics

Partitioning of interaction energy in van der Waals complexes involving excited state species: The $He(^1S)+Cl_2(B\ ^3\Pi_u)$ interaction

Sławomir M. Cybulski
Department of Chemistry, Oakland University, Rochester, Michigan 48309 and Department of Chemistry, Miami University, Oxford, Ohio 45056[a)]

Rudolf Burcl
Department of Chemistry, Oakland University, Rochester, Michigan 48309

Grzegorz Chałasiński
Department of Chemistry and Biochemistry, Southern Illinois University, Carbondale, Illinois 62901 and Department of Chemistry, University of Warsaw, Pasteura 1, 02-093 Warszawa, Poland[a)]

M. M. Szczęśniak
Department of Chemistry, Oakland University, Rochester, Michigan 48309

(Received 14 June 1995; accepted 8 September 1995)

The partitioning of interaction energy between a closed-shell and an open-shell system is proposed. This allows us to describe the unrestricted Møller–Plesset interaction energy as a sum of fundamental contributions: electrostatic, exchange, induction and dispersion. The supermolecular energies derived within unrestricted Møller–Plesset perturbation theory are analyzed in terms of perturbation theory of intermolecular forces. The latter has been generalized to allow for the description of monomer wave functions within the unrestricted Hartree–Fock approach. The method is applied to the potential energy surfaces for the first excited triplet states, $^3A'$ and $^3A''$, of the $He+Cl_2(^3\Pi_u)$ complex. The $^3A'$ and $^3A''$ potential energy surfaces have different shapes. The lower one, $^3A'$, has a single minimum for the T-shaped structure. The higher one, $^3A''$, has the global minimum for the T-shaped structure and the secondary minimum for a linear orientation. The calculated well depth for the $^3A'$ state is 31.1 cm^{-1} at the 3.75 Å intersystem separation at the UMP2 level with extended basis set involving bond functions. The $^3A''$ well depth is approximately 2.3 cm^{-1} smaller at this level. This order is reversed by higher correlation effects. The angular and radial behaviors of the individual components of the $^3A'$ and $^3A''$ interaction energies are compared to reveal the different nature of interaction energies in both states. A comparison with the ground state reveals that the A'' state has a typical van der Waals character similar to that of the ground state. The A' state, on the other hand, differs considerably from the ground state. The A' and A'' states differ primarily in different role of the intramonomer correlation effects. © *1995 American Institute of Physics.*

I. INTRODUCTION

Since the seminal work of Smalley, Levy, and Wharton,[1] the dynamics of the rare gas–halogen molecules has served as an important model problem for understanding both vibrational and electronic coupling (cf. Jahn *et al.*[2] and references therein). The rare gas–halogen species belong to the simplest van der Waals complexes besides the rare gas dimers. Yet, there are many intriguing questions about their structure and bonding. First, for most van der Waals clusters, the van der Waals bond is stronger in the valence excited electronic state than in the ground state. This may be attributed to an increase of the polarizability upon electron excitation. In contrast, in rare gas–halogen molecules the van der Waals bonding becomes weaker upon excitation to the *A* and *B* electronic states. Another interesting problem is the ''structure'' of the rare gas–halogen molecule complexes. For some species, the position of the global minimum on the *ab initio* potential energy surface (PES) coincides with the empirical prediction. These are the cases of the linear form of Ar–ClF[3–5] and the T-shaped form of $He–Cl_2(^3\Pi_u)$.[6–8] For others, such as the ground states of $Ar–Cl_2$ and $He–Cl_2$, the spectroscopic results indicate the T-shaped form (Refs. 6 and 7, respectively) whereas the *ab initio* results indicate that the T-shape structure is a *secondary* minimum, and the global minimum occurs for the collinear arrangement (Refs. 4 and 8, and 9, respectively). The latter discrepancy has recently been resolved in the case of $He–Cl_2$. Huang *et al.*[6(d)] have shown that even when the potential energy surface has the global minimum for linear configuration the ground vibrational state probability peaks around the T structure. This astonishing result indicates that the understanding of the structure and dynamics of rare gas–halogen species demands high quality calculations of the PESs combined with an advanced treatment of vibrational dynamics.

In a series of recent papers, we, as well as other researchers, undertook *ab initio* studies of the PESs for several rare gas–halogen van der Waals species: Ar–ClF,[4,5] $Ar–Cl_2$,[4,9] $He–Cl_2$.[8] The focus of this effort was essentially on the ground states. However, there is also a great deal of interest in the *B* excited states of these species. They are related to the long-lived $B\ ^3\Pi_{0^+u}$ electronic state of Cl_2, the

[a)]Permanent address.

 0021-9606/95/103(23)/10116/12/$6.00

vibrational predissociation dynamics of which has been extensively studied by the pump–probe spectroscopy.[6(a)] Therefore, in our recent paper on He–Cl_2 we used the unrestricted Møller–Plesset perturbation theory (UMPPT) to provide a preliminary characterization of two, closely spaced excited triplet states, $^3A'$ and $^3A''$, related to the He(^1S)–Cl_2($^3\Pi_u$) interaction. A splitting of the double degeneracy of the molecule in a Π electronic state is caused by the approach of an atom. The overall symmetry is lowered to the C_s group and leads to two electronic states whose functions have A' and A'' reflection symmetry in the triatomic plane. Unfortunately, we could not obtain complete PESs of the A' and A'' states due to persistent difficulties with symmetry breaking in the unrestricted Hartree–Fock formalism. In the previous paper, we presented only a limited selection of points on the A' PES and calculated only the T-shaped form of the A'' state. Both states revealed a T-shaped structure as the global minimum in contrast to the ground state where the linear form was more stable. The best estimate of the global minimum well depth was 30 cm^{-1}, for the T-shaped A'', which agrees with the experimental estimate.[6(c)] We also showed that the electron density in the excited state is convex rather than concave at the terminal Cl atoms. On the other hand, some details turned out somewhat disturbing. For example, the A'' state was lower in energy than the A', whereas in the literature for similar interactions between rare-gas atom and Π-state diatom, the A'' state was found slightly higher (Ar–NO,[10] He–NH,[11] Ar–OH,[12]) which is in agreement with simple intuition that the repulsive effects due to the doubly occupied π orbital should be larger than for the singly occupied π orbital.

A more complete and accurate description of the A' and A'' PESs is clearly warranted. Moreover, so far only supermolecular calculations were carried out which provided a limited insight into physical origin of the interaction. To this end, in this paper we derived and implemented the intermolecular unrestricted Møller–Plesset perturbation theory (I-UMPPT) applicable to open-shell systems. It is a generalization of the intermolecular-MPPT, a symmetry-adapted perturbation formalism for interaction of closed shell systems, based on the Møller–Plesset zero-order Hamiltonian.[13–16] I-UMPPT provides dissection of the interaction energy into fundamental components: electrostatic, exchange, induction, dispersion, in a manner parallel to the closed-shell case.[17–19] This approach also proved helpful in ensuring the desired state and symmetry in the supermolecular calculations. Consequently, we were able to calculate the PESs for both the A' and A'' states for a wide range of intermolecular distances and complete set of angles.

II. METHOD AND DEFINITIONS

The supermolecular Møller–Plesset perturbation theory (MPPT), both for closed- and open-shell states, derives the interaction energy corrections as the differences between the values for the total energy of the dimer and the sum of the subsystem energies in every order of perturbation theory

$$\Delta E^{(n)} = E_{AB}^{(n)} - E_A^{(n)} - E_B^{(n)} \quad n = \mathrm{UHF}, 2, 3, 4, \ldots . \tag{1}$$

The sum of corrections through the nth order will be denoted $\Delta E(n)$; thus, e.g., $\Delta E(3)$ will symbolize the sum of ΔE^{UHF}, $\Delta E^{(2)}$, and $\Delta E^{(3)}$.

In the case of closed-shell monomers, each $\Delta E^{(n)}$ correction can be interpreted[17–19] in terms of intermolecular Møller–Plesset perturbation theory (I-MPPT). I-MPPT is a symmetry adapted perturbation theory (SAPT) developed for the Møller–Plesset partitioning of the dimer Hamiltonian.[13–16] I-MPPT encompasses all well defined and meaningful contributions to the interaction energy such as electrostatic, induction, dispersion and exchange, which are expressed in the form of a double perturbation expansion.[16] Generalization of the closed-shell formalism to open-shell systems described by unrestricted MPPT (UMPPT) essentially requires a separate treatment of each spin case. The related I-UMPPT interaction energy corrections are denoted as $\epsilon^{(ij)}$, where i and j refer to the order of the intermolecular interaction operator and the intramolecular correlation operator, respectively (see Ref. 14 for more details on the closed-shell case).

The use of UMPPT in describing monomers and the dimer causes new problems. First, the resulting open-shell states are no longer pure spin states. This is not serious as long as the spin contamination is small and practically identical for both the dimer and the open-shell monomer(s). Another commonplace difficulty is that not only may the UHF procedure fail to converge, but it may converge to a symmetry-breaking solution or to a different state that was initially intended.

A. Partitioning of ΔE^{UHF}

ΔE^{UHF} can be dissected as follows:

$$\Delta E^{\mathrm{UHF}} = \Delta E^{\mathrm{HL}} + \Delta E_{\mathrm{def}}^{\mathrm{UHF}}, \tag{2}$$

where ΔE^{HL} and $\Delta E_{\mathrm{def}}^{\mathrm{UHF}}$ are the Heitler–London and UHF-deformation contributions, respectively. ΔE^{HL} is given after Löwdin[20(a)] as

$$\Delta E^{\mathrm{HL}} = \frac{\langle \mathscr{A}AB|H|\mathscr{A}AB\rangle}{\langle \mathscr{A}AB|\mathscr{A}AB\rangle} - \frac{\langle A|H_A|A\rangle}{\langle A|A\rangle} - \frac{\langle B|H_B|B\rangle}{\langle B|B\rangle}, \tag{3}$$

where $\mathscr{A}$ is the antisymmetrizer for the dimer, A and B are the unrestricted Hartree–Fock wave functions of the monomers denoted by the same letters; H, H_A, and H_B are the dimer and monomer Hamiltonians, respectively. Since the product AB is subjected to the antisymmetrization, the energy does not depend on either inter- or intramonomer unitary linear transformations. Therefore, the unrestricted orbitals may be conveniently orthogonalized in any order, and the matrix element routinely calculated. This property has also been confirmed in actual calculations. This is an important feature of the unrestricted wave function. In contrast, the restricted Hartree–Fock solutions for open-shell monomers would provide the matrix element of H which, in general, is not invariant with respect to arbitrary orthogonalization procedures as pointed out in Refs. 21 and 22.

ΔE^{HL} is further divided into the electrostatic, $\epsilon_{\mathrm{es}}^{(10)}$, and exchange, $\epsilon_{\mathrm{exch}}^{\mathrm{HL}}$, components

$$\epsilon_{\rm es}^{(10)}=\langle AB|V|AB\rangle, \tag{4}$$

$$\epsilon_{\rm exch}^{\rm HL}=\Delta E^{\rm HL}-\epsilon_{\rm es}^{(10)}. \tag{5}$$

It should be mentioned here that the first-order exchange energy may also be defined strictly within the framework of SAPT.[14,20(b)] It is then denoted $\epsilon_{\rm exch}^{(10)}$. It differs from $\epsilon_{\rm exch}^{\rm HL}$ by terms of the fourth order with respect to the intermolecular overlap, in general a safely negligible quantity, provided the UHF wave functions of monomers are obtained with the basis set of the full dimer.[23]

The UHF-deformation defined by Eq. (2) originates from the mutual electric polarization restrained by the Pauli principle (quantum exchange effects).[24] In this sense, $\Delta E_{\rm def}^{\rm UHF}$ may be viewed as *the quantum induction effect*. Two exchangeless approximations to $\Delta E_{\rm def}^{\rm UHF}$ are also considered here: which are $\epsilon_{\rm ind}^{(20)}$ and $\epsilon_{{\rm ind},r}^{(20)}$. They may be viewed as *the classical induction effects*. The former describes the second-order induction effect at the uncoupled Hartree–Fock (UCHF) level, while the latter at the coupled Hartree–Fock (CHF) level (''r'' denotes inclusion of response effects).[25] As with other components of the interaction energy, $\epsilon_{\rm ind}^{(20)}$ and $\epsilon_{{\rm ind},r}^{(20)}$ have not been reported so far for an open-shell complex.

B. Partitioning of $\Delta E^{(2)}$

As with the closed-shell case, the second-order supermolecular UMPPT interaction energy can be partitioned as follows:

$$\Delta E^{(2)}=\epsilon_{{\rm es},r}^{(12)}+\epsilon_{\rm disp}^{(20)}+\Delta E_{\rm def}^{(2)}+\Delta E_{\rm exch}^{(2)}, \tag{6}$$

where $\epsilon_{{\rm es},r}^{(12)}$ denotes the second-order electrostatic correlation energy with response effects and $\epsilon_{\rm disp}^{(20)}$ the second-order unrestricted Hartree–Fock dispersion energy. The remaining terms, $\Delta E_{\rm def}^{(2)}$ and $\Delta E_{\rm exch}^{(2)}$, describe, respectively, the second-order deformation correlation correction to the UHF deformation and the second-order exchange correlation. $\Delta E_{\rm exch}^{(2)}$ encompasses the exchange-correlation effects related to electrostatic correlation and dispersion. If the deformation-correlation contribution is negligible it can be extracted from Eq. (6)

$$\Delta E_{\rm exch}^{(2)}\cong\Delta E^{(2)}-\epsilon_{\rm disp}^{(20)}-\epsilon_{{\rm es},r}^{(12)}. \tag{7}$$

C. I-MPPT component energies

In giving the detailed expressions for the component energies we will follow a common convention and use symbols $i,j,k,\ldots$ for occupied, and $a,b,c,\ldots$ for virtual molecular spin orbitals. For nuclei, we will use symbols $I,J,\ldots$ and for atomic orbitals we will use symbols μ and ν. Finally, for monomers, we will use symbols A and B. All formulas for component energies for open-shell interactions considered here are based on the unrestricted Hartree–Fock (UHF) procedure and may be viewed as generalizations of the appropriate formulas developed by others for closed-shell interactions. The expression for the first-order interaction energy for a closed-shell dimer has been given by Jeziorski *et al.*[20(b)] For an open-shell dimer, the related expression has the form

$$E^{(10)}=\sum_{I\in A}\sum_{J\in B}\frac{Z_IZ_J}{R_{IJ}}+\sum_{i\in A}\sum_{j}D_{ji}(i|U_B|j)+\sum_{i\in B}\sum_{j}D_{ji}(i|U_A|j)+\sum_{i\in A}\sum_{j\in B}\sum_{k}\sum_{l}D_{ki}D_{lj}[(ik|jl)-(il|jk)]. \tag{8}$$

The first term is the repulsion energy between nuclei, the second and third one are the Coulomb attraction energies between electrons and nuclei, and the fourth one is the repulsion energy between electrons. All four terms represent only intermolecular interactions. $U_A(U_B)$ in Eq. (8) denotes the nuclear attraction energy operator for nucleus $A(B)$. For the ith electron, it is given by

$$U_A=-\sum_{I\in A}\frac{Z_I}{r_{Ii}}. \tag{9}$$

Density matrices in Eq. (8) are denoted by D and can be obtained by inverting the intermolecular overlap matrix.[20(b)] For each monomer, it is possible to decompose $D^{20(b)}$ into the unperturbed density matrix, $D^{(0)}$, and the exchange density matrix, $D^{\rm exch}$

$$D=D^{(0)}+D^{\rm exch}. \tag{10}$$

The latter one vanishes in the limit of infinite intermolecular separation. The first-order interaction energy is the sum of the first-order electrostatic and exchange energies

$$E^{(10)}=\epsilon_{\rm es}^{(10)}+\epsilon_{\rm exch}^{(10)}. \tag{11}$$

The first-order electrostatic energy can be evaluated from Eq. (8) if the exchange part of the density matrix is neglected,

$$\epsilon_{\rm es}^{(10)}=\sum_{I\in A}\sum_{J\in B}\frac{Z_IZ_J}{R_{IJ}}+\sum_{i\in A}(i|U_B|i)+\sum_{i\in B}(i|U_A|i)+\sum_{i\in A}\sum_{j\in B}(ii|jj). \tag{12}$$

As we mentioned earlier, the first-order interaction energy given by Eq. (8) differs from the Heilter–London energy given by Eq. (3) by terms proportional to the fourth order with respect to the intermolecular overlap.[20(b),23] It is convenient to include such terms in the exchange interaction energy which is then termed ''HL-exchange energy.'' Then, Eq. (11) may then be rewritten as

$$\Delta E^{\rm HL}=\epsilon_{\rm es}^{(10)}+\epsilon_{\rm exch}^{\rm HL}. \tag{13}$$

The second-order coupled induction energy was evaluated from the following expression:

$$\epsilon_{{\rm ind},r}^{(20)}=\sum_{\nu\mu}D_{A,\nu\mu}^{(10)}(\mu|V_B|\nu)+\sum_{\nu\mu}D_{B,\nu\mu}^{(10)}(\mu|V_A|\nu), \tag{14}$$

where $D_{A,\nu\mu}^{(10)}$ and $D_{B,\nu\mu}^{(10)}$ denote the elements of the appropriate first-order CHF perturbed density matrices. They can be obtained by solving the first-order CHF equations with the perturbation matrix whose elements are defined by

$$(\mu|V_X|\nu)=(\mu|U_X|\nu)+\sum_{i\in X}(\mu\nu|ii). \tag{15}$$

By replacing the CHF density matrices in Eq. (14) with their uncoupled Hartree–Fock (UCHF) counterparts (equivalent to the zeroth-order iteration of the CHF procedure), the second-order induction energy without response effects, $\epsilon_{\rm ind}^{(20)}$, can be evaluated.

As with the electrostatics, exchange and induction the second-order dispersion energy for open-shell dimers is simply a generalization of the formula for closed-shell dimers[20(c)]

$$\epsilon_{\rm disp}^{(20)}=\sum_{i\in A}\sum_{j\in B}\sum_{a\in A}\sum_{b\in B}\frac{\langle ij|ab\rangle\langle ab|ij\rangle}{\epsilon_i+\epsilon_j-\epsilon_a-\epsilon_b}. \tag{16}$$

Finally, the second-order electrostatic correlation energy energy with response effect, $\epsilon_{{\rm es},r}^{(12)}$, was evaluated from the formula

$$\epsilon_{{\rm es},r}^{(12)}=\sum_{\nu\mu}D_{A,\nu\mu}^{(02)}(\mu|V_B|\nu)+\sum_{\nu\mu}D_{B,\nu\mu}^{(02)}(\mu|V_A|\nu), \tag{17}$$

where $D_{A,\nu\mu}^{(02)}$ and $D_{B,\nu\mu}^{(02)}$ denote the elements of the appropriate second-order intramonomer correlation correction to the zeroth-order density matrices frequently refered to as ''relaxed'' density matrices. Detailed formulas leading to the evaluation of these matrices have been given by Salter *et al.*[20(d)]

The main difficulties of the open-shell partitioning of the interaction energy are related to a necessity of separate calculations for each nonvanishing spin combination, and the coupling between the two spin cases. In the case of dispersion energy, there are four nonvanishing spin combinations that need to be evaluated: $(\alpha\alpha|\alpha\alpha)$, $(\alpha\alpha|\beta\beta)$, $(\beta\beta|\alpha\alpha)$, and $(\beta\beta|\beta\beta)$. In the case of induction and electrostatic correlation energies, the equations involving α and β spin forms of various matrices are coupled.

D. Calculations of interaction energies

Calculations of all the supermolecular ΔE values and perturbational interaction terms $\epsilon^{(ij)}$ were performed using the basis set of the entire complex, i.e., dimer-centered basis sets (DCBS).[26,27] With reference to supermolecular quantities this procedure amounts to applying the counterpoise method of Boys and Bernardi.[28] To assure the consistency of evaluation of the UMPPT and I-UMPPT interaction energy corrections, all the intermolecular perturbation terms, $\epsilon^{(ij)}$, must be derived in DCBS as well.

In contrast to interactions between closed-shell states, the counterpoise procedure for open-shell states causes an additional complication. For example, the calculation of the Π symmetry state of Cl_2 with ghost orbitals located as in the T-shaped geometry lowers the cylindrical symmetry of the Cl_2 molecule, and, similarly to the dimer, yields $^3A'$ and $^3A''$ monomer states. In our previous work,[8] we used the same correction for both states because, at that time, we were unable to produce both corrections due to difficulties in forcing desired symmetry. We also expressed some doubts whether a consistent treatment really demanded two reference monomer energies. However, in similar studies of the rare-gas atom–Π state radical interactions (Ar–NO,[10] He–CN,[29] He–NH,[11] and Ar–OH[12]) the authors evaluated a different CP correction for each state. In the present work we also followed this approach. We found that it provides much more reasonable results. Consequently, in contrast to our previous study,[8] the $^3A'$ state became more attractive than $^3A''$. Also, the $A'-A''$ splitting has been reduced.

Another problem when applying UMPPT is spin contamination. In all the supermolecular and perturbation calculations the spin contamination of both the Cl_2 moiety (calculated within DCBS) and the dimer was very small. For the Cl_2 monomer, S^2 was equal to 2.0427 for the MCBS and all DCBS calculations. For the dimer, S^2 oscillated from 2.0419 to 2.0429. Occasionally the UHF procedure for the dimer converged to an unwanted local minimum. This was manifested by S^2 different from the above values and equal to 2.0197. It is important to stress that both the dimer and monomer must have practically the same spin contamination. Otherwise, subtraction of the dimer and monomer energies becomes inconsistent and the interaction energies nonsensical.

The calculations were carried out using GAUSSIAN 92[30] programs and the new version of intermolecular perturbation theory package TRURL 94[31] which includes I-UMPPT corrections.

E. Basis sets and geometries

The basis sets used throughout this study were the same as those used previously[8] and were based on the following choice:

Cl:$(14s,10p,4d,1f)/[7s,5p,2d,1f]$ medium-polarized basis set constructed in Ref. 32 according to the prescription of Sadlej[33] augmented with one f-symmetry orbital (exponent 0.15); the quality of this basis set for Cl was also discussed in the paper on Ar–Cl_2.[9]

He:$(10s,6p,2d)/[6s,4p,2d]$. The $(10s6p)/[6s4p]$ part was taken from Gutowski *et al.*[34] (this set was used there in the HeLi+case). The d-symmetry functions (exponents: 0.152 93, 0.498 71) were optimized for dispersion term by Gutowski *et al.*[35]

Selected points on the PES were also calculated with a larger basis set, denoted $spdf(b\text{-ext})$ which included a set of bond functions $[3s3p2d]$ of Tao and Pan[36] (sp: 0.9, 0.3, 0.1; d: 0.6, 0.2). This set was originally designed for He_2, but has also proven very efficient in the calculations for other van der Waals complexes, provided the distortion of the electrostatic correlation is kept small.[19,37]

The definition of geometrical parameters of the He–Cl_2 complex is the same as in the previous paper (cf. Fig. 1 in Ref. 8): R denotes the distance between the center of mass of the Cl_2 molecule and the He atom, and Θ corresponds to the angle between the R vector and the Cl_2 bond axis. The interatomic separation in the $^3\Pi_u$ state was kept at 2.400 Å.[38] The excited Cl_2 molecule is in the lowest triplet state and thus can be treated by the UMPPT framework. Moreover, this state is well isolated from the ground and other excited states so no curve crossing occurs.[38] The spin contamination is very small and S^2 amounts to 2.0427. We also computed polariz-

TABLE I. PES of the $^3A'$ state of He–Cl_2 ($B\ ^3\Pi_u$) complex from the UMP2/$spdf$ level calculations in μH.

R (Å)	Θ(°): 0.0	20.0	40.0	60.0	80.0	90.0[a]
3.25				753.53	15.02	−40.34
3.50	8348.59		1536.48	160.12	−104.76	−122.48
3.75	3122.86	1943.45	456.83	−45.55	−122.9	−126.32
4.00	1058.2	608.63	60.53	−98.66	−107.55	−106.2
4.25	280.51	118.40	−64.75	−97.48	−85.15	−82.66
4.50	10.77	−41.72	−89.51	−80.76	−64.67	−62.32
4.75	−67.15	−79.73	−81.27	−62.60	−48.39	−46.49
5.00	−77.43	−76.72	−65.26	−47.26	−36.12	−34.68
5.25	−67.09	−62.87	−49.97	−35.42	−27.08	−26.03
5.50	−52.96	−48.58	−37.62	−26.59	−20.46	−19.72

[a]A Morse fit yields the following minimum parameters, R_e=3.64 Å and the well depth is 129.64 μH.

abilities of Cl_2 in the $^3\Pi_u$ state. For the y component of the $^3\Pi_u$ state (related to configuration $\pi_x\pi_y^2$) at the UHF level we obtained: α_{zz}=83.068 a.u., α_{xx}=26.972 a.u., and α_{yy}=26.198 a.u. At the UMP2 level they are only slightly different: α_{zz}=81.985 a.u., α_{xx}=27.792 a.u., and α_{yy} =27.300 a.u. The difference between α_{xx} and α_{yy} is a result of lowering symmetry to A' and A'', respectively, once the electric field is applied to the Π_u state of Cl_2. The excited state polarizability components may be compared with those of the ground state. The ground state components α_{xx} and α_{yy} are equal, and amount to 23.749 a.u. at the RHF level and to 25.338 a.u. at the MP2 level. The perpendicular components are thus similar in the ground and the excited state. The α_{zz} component, however, is two times smaller in the ground state (42.303 a.u. at the RHF and 42.056 a.u. at the MP2 level). It appears that this difference is partially due to the elongation of the Cl–Cl bond which occurs in the excited state and partially due to promoting one electron to a σ^* orbital. For example, when the ground state Cl–Cl distance is stretched accordingly, we obtained 67.318 a.u. for α_{zz} (RHF). The α_{xx} and α_{yy} components remain almost the same 25.500 a.u. (RHF) upon stretching. To summarize, compared to the ground state, the excited state is substantially more polarizable along the Cl–Cl bond and slightly more polarizable perpendicular to the bond. The increase of polarizability is due to rearrangement of the electron density. This rearrangement is also reflected by the magnitude of the quadrupole moment Θ_{zz}. At the RHF level, for the ground state Θ_{zz} equals 3.203 B. Since it is positive, the chlorine ends reveal relative electron depletion compared to the midbond region. This depletion is enhanced when the Cl–Cl bond is stretched (at $R_{\mathrm{Cl-Cl}}$=2.4 Å Θ_{zz}=4.689 B). On the other hand, for the $^3\Pi_u$ state Θ_{zz}=1.406 B. In view of the fact that Θ_{zz} is reduced in the excited state, the relative electron depletion at the terminal atoms has been considerably reduced.

III. RESULTS AND DISCUSSION

A. Features of total PES

The interaction energies for $^3A'$ and $^3A''$ states are reported in Tables I and II. They were obtained at the UMP2 level of theory, for a wide range of intermolecular distances, from 3.25 to 5.50 Å, and for angles from 0° to 90°. The curves representing angular cuts across the $^3A'$ PES are also shown: in Fig. 1(a) (R=3.25–4.25 Å), and in Fig. 1(b) (R =4.50–5.50 Å). Since the A'–A'' splitting is small in comparison with the interaction energy of both states, we have not provided separate figures for $^3A''$. The characteristics of the global minima at the UMP2 level (see Table III) are as follows. $^3A'$: D_e=27.7 cm^{-1}, R_e=3.75 Å, and $^3A''$: D_e=26.3 cm^{-1}, R_e=3.75 Å. The global minimum for the $^3A'$ state appears to be deeper than that of the $^3A''$ state only by about 1.5 cm^{-1}. However, at the UMP4/$spdf$ level the relative stability of both minima is reversed (see Table III). The well depth of the $^3A'$ minimum is ca. 27.8 cm^{-1} whereas that of A'' is 29.0 cm^{-1}. More discussion on this subject will be provided below.

TABLE II. PES of the $^3A''$ state of He–Cl_2 ($B\ ^3\Pi_u$) complex from the UMP2/$spdf$ level calculations in μH.

R (Å)	Θ(°): 0.0	20.0	40.0	60.0	80.0	90.0[a]
3.25				1254.96	48.55	−51.64
3.50	8348.59		2262.65	399.22	−81.12	−119.76
3.75	3122.86	2228.59	783.00	67.51	−107.04	−120.02
4.00	1058.2	732.26	205.21	−45.23	−97.2	−100.16
4.25	280.51	171.17	−0.98	−72.01	−78.44	−77.85
4.50	10.77	−19.35	−61.41	−68.38	−60.34	−58.82
4.75	−67.15	−70.26	−68.78	−56.37	−45.56	−44.01
5.00	−77.43	−72.68	−59.57	−43.99	−34.24	−32.97
5.25	−67.09	−61.14	−47.29	−33.56	−25.82	−24.84
5.50	−52.96	−47.78	−36.26	−25.49	−19.62	−18.88

[a]A Morse fit yields the following minimum parameters, R_e=3.619 Å, and the well depth is 124.33 μH.

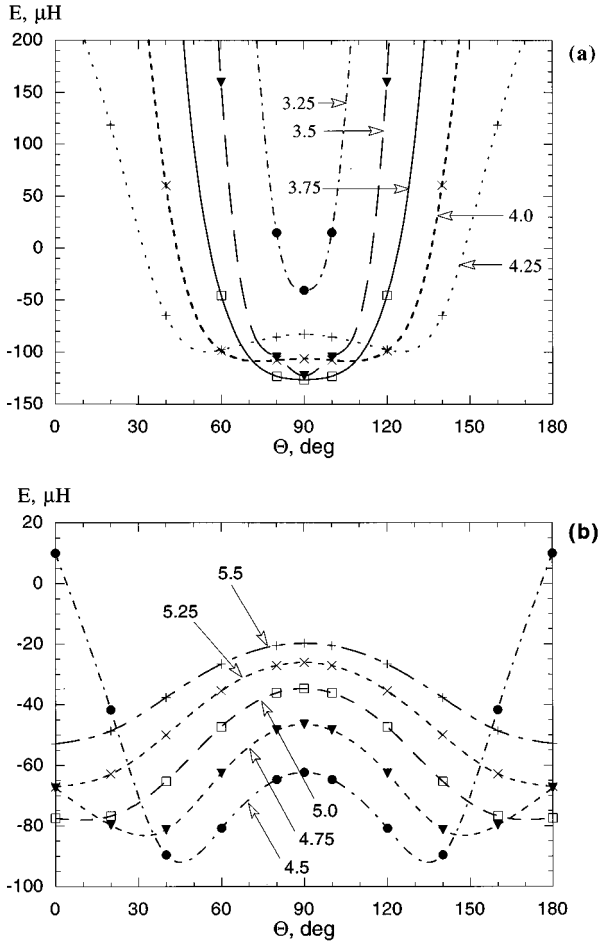

FIG. 1. Potential energy surface for the A' state of the He–Cl_2 ($B\ ^3\Pi_u$) complex at the UMP2/$spdf$ level; (a) R=3.25–4.25 Å distances, (b) R=4.5–5.5 Å distances.

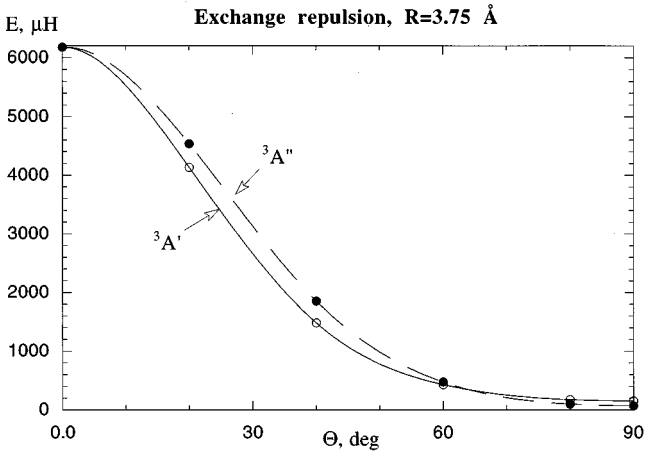

FIG. 2. Comparison of $\epsilon_{\rm exch}^{\rm HL}$ in two states A' and A'' of the He–Cl_2 ($B\ ^3\Pi_u$) complex at R=3.75 Å.

Interestingly, the two PESs have distinctly different topologies. For example, the $^3A'$ surface has only one minimum for the T-shaped geometry while the $^3A''$ surface has a global minimum for the T structure and a secondary minimum for the collinear geometry. The latter geometry serves as a saddle point at the $^3A'$ PES. The characteristics for this geometry are R_e=5.0 Å and D_e=17.0 cm^{-1}, in agreement with the previous work.[8] The barrier separating the two minima at the $^3A''$ surface is very small, ca. 1.9 cm^{-1}, for a passage from the linear to T configuration.

Comparison of Tables I and II indicates that the $^3A''$ state lies above the $^3A'$ state except for intersystem distances R shorter than 3.5 Å at Θ=90° where the two states switch. The gap between the states is maximal for angles 60°–40° and for the linear arrangement Θ=0° the states converge. The differences reflect the different position of He with respect to the doubly occupied π^* orbital of Cl_2. A more detailed analysis of this effect will be provided below.

TABLE III. Minimum energy characteristics (in μH) of the excited state He–Cl_2 ($B\ ^3\Pi_u$) complex (frozen-core approximation) using the $spdf$ basis set unless stated otherwise.[a]

	Linear, (R=5,0 Å, Θ=0°)	T, (R=3.75 Å, Θ=90°)	
	$^3\Pi$	$^3A'$	$^3A''$
$\Delta E^{\rm UHF}$	43.80 (43.92)	108.16 (110.1)	49.22 (49.7)
$\Delta E^{(2)}$	−121.23	−234.48	−169.24
$\Delta E(2)$	−77.43 (−83.06)	−126.32 (−141.9)	−120.02 (−131.3)
$\Delta E^{(3)}$		7.7	−1.0
$\Delta E^{(4)}$		−8.4	−11.6
$\Delta E(4)$		−127.0	−132.6
$\epsilon_{\rm exch}^{\rm HL}$	61.18	153.07	68.55
$\epsilon_{\rm es}^{(10)}$	−11.31	−27.65	−13.1
$\Delta E_{\rm def}^{\rm UHF}$	−6.07	−17.26	−6.23
$\epsilon_{\rm ind}^{(20)}$	−3.46	−9.35	−3.62
$\epsilon_{{\rm ind},r}^{(20)}$	−3.87	−10.54	−4.08
$\epsilon_{{\rm es},r}^{(12)}$	−4.38	9.19	−6.32
$\epsilon_{\rm disp}^{(20)}$	−138.51	−213.59	−194.75
$\Delta E_{\rm exch}^{(2)}$	21.66	−30.08	31.83
$\Delta E^{\rm UHF}+\epsilon_{\rm disp}^{20}$	−94.71	−105.4	−145.53
$\Delta E^{\rm HL}+\epsilon_{\rm disp}^{(20)}$	−88.64	−88.17	−139.3

[a]Values in parentheses correspond to the $spdf$ basis set augmented with bond functions (see the text).

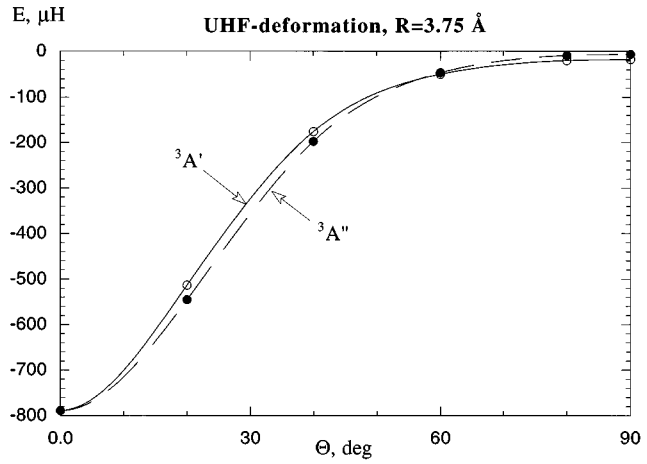

FIG. 3. Comparison of $\Delta E_{\mathrm{def}}^{\mathrm{UHF}}$ in two states A' and A'' of the He–Cl_2 ($B\ ^3\Pi_u$) complex at $R=3.75$ Å.

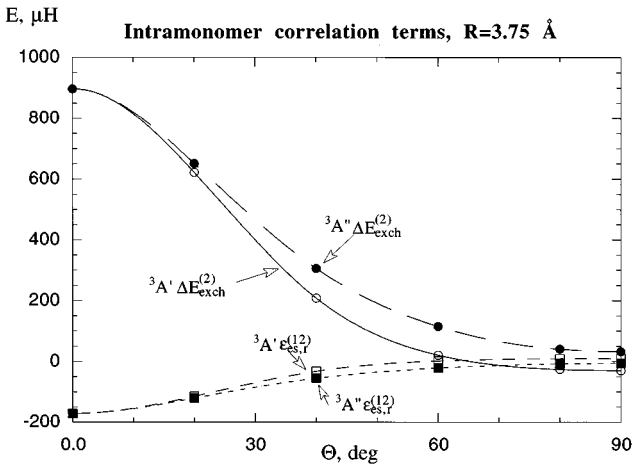

FIG. 5. Comparison of the intramonomer correlation effects, $\epsilon_{\mathrm{es,r}}^{(12)}$ and $\Delta E_{\mathrm{exch}}^{(2)}$, in two states A' and A'' of the He–Cl_2 ($B\ ^3\Pi_u$) complex at $R=3.75$ Å.

B. Decomposition of the interaction energy

The angular dependence of the perturbation components of interaction energy of both states at $R=3.75$ Å and the comparison of $^3A'$ and $^3A''$ states is presented in Figs. 2–5.

1. HL exchange

The HL-exchange term (Fig. 2) displays strong angular dependence with a minimum at 90° and maxima at 0° (and at 180°, not shown in Fig. 2). The overall growing repulsion for both states, from 90° to 0° is caused by the obvious fact that the electron density in the middle of the bond is ''thinner'' than at the atoms. This behavior is similar to that of the ground state studied previously.[8] Yet, in contrast to the ground state, there are no local minima on the molecular axis at the Cl ends. This suggests that there is no electron density depletion at the terminal atoms and the shape of the electron density for the excited states is convex. This is also reflected by the electrostatic term, $\epsilon_{\mathrm{es}}^{(10)}$ which is of a purely charge-overlap nature in the $HeCl_2$ case. One may expect that the change from a concave shape in the ground state to a convex shape in the excited state is due to the elongation of the Cl–Cl distance which occurs in the excited state. This, however, is not the case, since the stretch of Cl–Cl up to the equilibrium excited state separation did not affect the ground state HL-exchange energy. The main reason a depletion vanishes is the reorganization of the electron configuration of Cl_2 from π^4 to $\pi^3\sigma^*$.[8]

Comparison of the HL-exchange energy in the region around the middle of the Cl–Cl bond is also quite interesting. We found that the A'' exchange repulsion resembles that of the ground state quite closely for angles 60°–90°. (The agreement was even better when the ground state Cl–Cl distance was stretched to simulate the excited state equilibrium separation). At the same time, the A' state exchange repulsion in the same region is distinctly larger than both the ground state and the A'' state exchange repulsion.

Although the anisotropies of the $^3A'$ and $^3A''$ HL-exchange terms are qualitatively similar, as seen in Fig. 2, the HL-exchange of the A'' state is less repulsive at 90°, but when the angle decreases, it rises faster than for the A' state. Consequently, $\epsilon_{\mathrm{exch}}^{\mathrm{HL}}$ of the A' and A'' states cross one another at about 60° and past this point (in the range 60°–20°) the A'' term is more repulsive. The difference disappears at 0° where the two states converge. Similar features were observed for the larger R as well; the crossing point shifted, however, to 50° at $R=5.0$ Å.

The fact that the A'' HL-exchange becomes more repulsive for intermediate angles (60°–20°) may be explained by analyzing the orientation of He with respect to the doubly and singly occupied π^* orbitals of Cl_2. In the A' state, He lies in the same plane as the singly occupied π^* orbital, whereas in A'' it lies in the plane of the doubly occupied π^* orbital. It is clear that the He atom will be more repelled by the doubly occupied orbital (as anticipated in Ref. 8). This indeed explains what happens in the region 0°–60°. But why is HL-exchange repulsion *smaller* for the A'' state than for the A' in the vicinity of 90°, i.e., when He approaches the nodal plane perpendicular to the Cl_2 bond axis? This fact eludes simple rationalization.

In view of the above, the $^3\Pi_u$ state of Cl_2 may be visualized as an ellipsoidal dumbbell. Compared to the ground

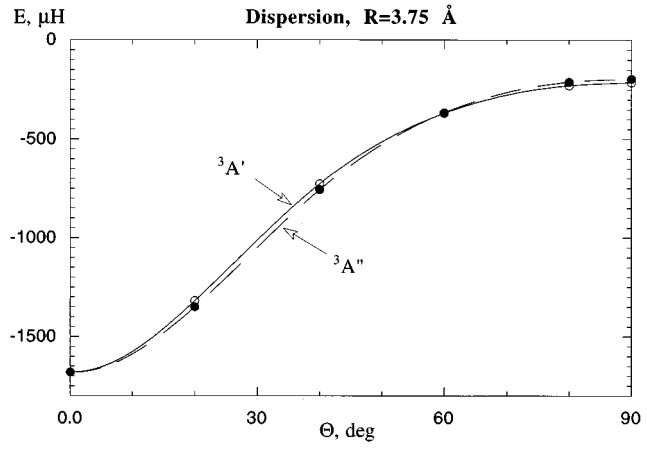

FIG. 4. Comparison of $\epsilon_{\mathrm{disp}}^{(20)}$ in two states A' and A'' of the He–Cl_2 ($B\ ^3\Pi_u$) complex at $R=3.75$ Å.

state, the dumbbell is ''thicker'' in the middle of the Cl–Cl bond and its ends are convex. The differences between $^3A'$ and $^3A''$ also suggest that ''the singly occupied side'' of excited Cl_2 protrudes less than the ''doubly occupied side.''

2. UHF-deformation and induction terms

The UHF-deformation (cf. Fig. 3) behaves in the opposite manner to the HL-exchange, that is, for both states it has a maximum at 90° and a minimum at 0°. Detailed comparison of the absolute values of the UHF-deformation terms for $^3A'$ and $^3A''$ (cf. Fig. 3) reveals a similar trend to the HL-exchange: the attraction at 90° is smaller for the A'' state, but it grows faster with the decreasing angle, crossing the A' state curve at 60°. The curves eventually coincide at 0°. The exchangless approximation to UHF-deformation, $\epsilon_{\mathrm{ind},r}^{(20)}$, (not shown in the Fig. 3) is reasonable and reproduces all the trends described above. To rationalize this behavior one may use similar arguments about the interaction of He with either the doubly or singly occupied π^* orbital as those presented for the HL-exchange and the UHF-deformation terms. Similarly, a somewhat larger induction attraction of the $^3A'$ state at 90° seems to reflect the fact that for the y component of the $^3\Pi_u Cl_2$ state the α_{xx} polarizability component slightly exceeds α_{yy}, as if the singly occupied orbital were more diffuse in this direction than the doubly occupied one.

The above description is qualitatively valid also at the larger R, but the crossing point shifts to somewhat lower angles (at 5.0 Å it is about 50°).

Comparison with the ground state reveals that both the $^3A'$ and $^3A''$ UHF-deformation and induction energies are more attractive even in the middle of the Cl–Cl bond.

3. Dispersion

At 3.75 Å the dispersion energy (see Fig. 4) behaves in the opposite manner to the HL-exchange term; i.e., for both states it has a maximum at 90° and a minimum at 0°. Comparison of the dispersion attraction for the $^3A'$ and $^3A''$ states (cf. Fig. 4) reveals a similar trend to the HL exchange: the dispersion effect at 90° is smaller for the $^3A''$ state, but it grows faster with the decreasing angle, crossing the $^3A'$ state curve at 60°. To rationalize this behavior, one may use similar arguments about the interaction of He and the π^* orbitals as those presented above for the HL-exchange and UHF-deformation terms. Similarly, a somewhat larger dispersion attraction of the $^3A'$ state at 90° seems to reflect the fact that for the y component of the $^3\Pi_u Cl_2$ state α_{xx} slightly exceeds α_{yy}.

The above description is qualitatively valid also at larger R, but the crossing point shifts to somewhat lower angles (at 5.0 Å it occurs at about 40°).

Comparison with the ground state reveals that both the $^3A'$ and $^3A''$ dispersion energies are more attractive even in the middle of the Cl–Cl bond.

4. Intramonomer correlation corrections, $\epsilon_{\mathrm{es},r}^{(12)}$ and $\Delta E_{exch}^{(2)}$

The electrostatic-correlation correction, $\epsilon_{\mathrm{es},r}^{(12)}$, is small if compared to major terms (see Fig. 5). In the present case, it is of purely charge-overlap nature since the He atom possesses no permanent moments. It increases in absolute value when the angle decreases from 90° to 0°. The $^3A'$ state correction lies above the $^3A''$ correction (cf. Fig. 5) for all angles that are different from 0°. Interestingly, while $\epsilon_{\mathrm{es},r}^{(12)}$ is consistently negative for the $^3A''$ state, for the $^3A'$ state it is negative in the region 0°–60°, but positive in the region 60°–90°.

The second-order exchange-correlation part, $\Delta E_{\mathrm{exch}}^{(2)}$, is larger in absolute value than $\epsilon_{\mathrm{es},r}^{(12)}$ and varies with the angle in a reciprocal manner. The $^3A''$ state correction is consistently more repulsive.

It should be stressed that the intramonomer correlation corrections represent small adjustments to the uncorrelated fundamental terms. The anisotropy of correlation terms does not, and indeed needs not follow those of the uncorrelated terms, and their MO interpretation may be difficult. In the van der Waals minimum region at 3.75 Å, $\Delta E_{\mathrm{exch}}^{(2)}$ enhances the repulsion in the $^3A''$ state in comparison to the $^3A'$ state. $\epsilon_{\mathrm{es},r}^{(12)}$ acts in the opposite direction but is smaller in magnitude so the effect of $\Delta E_{\mathrm{exch}}^{(2)}$ is more important. Therefore, the latter term is responsible for the fact that the $^3A''$ state accumulates more repulsion with respect to the $^3A'$ state. Consequently, whereas the SCF and SCF+DISP approximations (not shown in the figures) faithfully follow the anisotropy of the HL-exchange component, the total UMP2 curves of $^3A'$ and $^3A''$ states do not. For instance, at 3.75 Å the UMP2 curves do not cross each other at 60°, and the $^3A'$ state lies consistently below the $^3A''$ state, (see the following section).

A larger magnitude of intramonomer correlation effect for $^3A''$ than for $^3A'$ could be caused by the fact that the $^3A''$ van der Waals bond engages an electron pair of Cl_2 rather than a single electron. In fact, the intramonomer correlation effect for $^3A''$ and for the ground state are very similar (some quantitative differences vanish upon stretching of the ground state Cl_2). The intramonomer correlation effect for the $^3A'$ state (with only a single electron directed toward He) differs considerably from both $^3A''$ and the ground state (e.g., it changes its sign around 60°).

C. Comparison of $^3A'$ and $^3A''$ PESs

To better visualize the difference between the $^3A'$ and $^3A''$ PESs, we plotted angular cuts at three separations $R=3.75$ Å (Fig. 6), 4.5 Å (Fig. 7), and 5.5 Å (Fig. 8). As expected, the shape at 3.75 Å (which is a relatively short R) is determined by the HL-exchange term, and the shape at 5.5 Å (which is a relatively large R)—by the dispersion term. The shape at 4.5 Å (which is an intermediate R) is a result of a more complicated balance between the attractive and repulsive components. The enhanced repulsion of the $^3A''$ state for angles 20°–60° is best visible for 3.75 and 4.5 Å. This is in agreement with the overall behavior of the HL-exchange term. However, the difference between the $^3A'$ and $^3A''$ states cannot be explained only by this term. Indeed, as shown in Fig. 2 the HL-exchange repulsion for the $^3A''$ state becomes larger than that for $^3A'$ at about 60° at each distance under consideration. Yet, at the UMP2 level of theory, the $^3A'$ state is consistently lower in energy than the $^3A''$ state with the exception of geometries with Θ in the vicinity of 90° and at the shortest $R=3.25$ Å. For these geometries the $^3A''$ state is lower in energy than $^3A'$. Interestingly, a similar crossing of

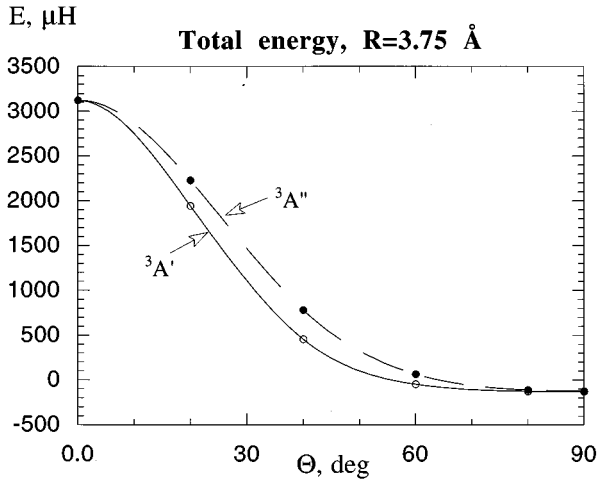

FIG. 6. Comparison of the Θ dependence of the A' and A'' states of the He–Cl_2 ($B\ ^3\Pi_u$) complex at $R=3.75$ Å (UMP2 level).

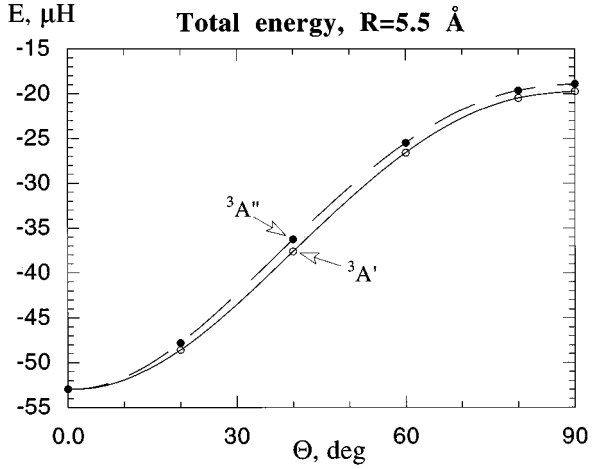

FIG. 8. Comparison of the Θ dependence of the A' and A'' states of the He–Cl_2 ($B\ ^3\Pi_u$) complex at $R=5.5$ Å (UMP2 level).

the $^3A'$ and $^3A''$ PES close to 90° was found for the Ar–NO ($X\ ^2\Pi$) complex.[10] This fact clearly shows that the interaction energy is balance of attractive and repulsive terms which often largely cancel (particularly in the region of van der Waals minimum) and predicting the final result by only qualitative comparison of fundamental components may be difficult. The short range rising of the $^3A'$ state above the $^3A''$ state at 90° is partly due to the competition of HL-exchange and dispersion terms, and partly due to differences in the intramonomer correlation effects in both states (cf. Fig. 5).

D. Convergence of S-UMPPT

To test the efficiency of the UMP2 treatment, we also carried out selected calculations at the UMP4 level. In Table III, we compare interaction energies for the $^3A'$ and $^3A''$ states for the T-shaped complex in the van der Waals minimum region ($R=3.75$ Å) through the fourth order of UMPPT. In agreement with our previous conclusions,[8] the perturbation expansions of the $^3A'$ and $^3A''$ states converge in a different way (see Table III). Namely, $\Delta E^{(3)}$ and $\Delta E^{(4)}$ are attractive for the $^3A''$ state, but cancel one another for the $^3A'$ state. The latter fact has important qualitative consequences: at the UMP2 level for $R=3.75$ Å the $^3A'$ state lies below $^3A''$, but at the UMP4 level the opposite is true. It seems that the crossing of the two states occurs at the UMP4 level at somewhat larger distances. The values of D_e for $^3A'$ and $^3A''$ at the UMP4 level are: 27.9 and 29.1 cm^{-1}, respectively. The related UMP2 values are 27.7 and 26.3 cm^{-1}, respectively.

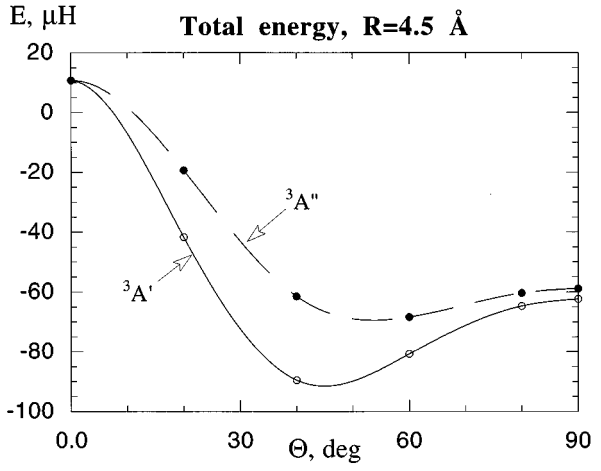

FIG. 7. Comparison of the Θ dependence of the A' and A'' states of the He–Cl_2 ($B\ ^3\Pi_u$) complex at $R=4.5$ Å (UMP2 level).

E. Basis set unsaturation effects

To assess the basis set unsaturation we carried out UMP2 calculations with the basis set which included bond functions, $spdf(b\text{-ext})$ (see Table III, values in parentheses). At the UHF level the changes are negligible. At the UMP2 level the changes are fairly small but significant: -3.4 and -2.4 cm^{-1} for the $^3A'$ and $^3A''$ states, respectively. The UMP2 values thus obtained are our best estimates of D_e for these two states and amount to 31.1 and 28.8 cm^{-1} for the $^3A'$ and $^3A''$ states, respectively. As discussed in the preceding section, higher order correlation effects may slightly increase these values.

F. Relevance to dynamics of He–Cl_2

The *ab initio* calculations reported in this paper are based on the Born–Oppenheimer approximation and thus provide the adiabatic PESs, $^3A'$ and $^3A''$. The actual scattering and spectroscopic experiments do not probe such states. To model the real dynamics of an open-shell complex, one has also to account for the spin–orbit coupling which leads to an interaction of different adiabatic states. A proper formalism for dynamic calculations has been set forth by Alexander[39] in the case of scattering states, and Dubernet, Flower, and Hutson[40] for bound states accessible by spectroscopy. In particular, in the case of bound states one needs to solve a set of coupled equations which results from the Schrödinger equation with effective Hamiltonian (which includes spin–orbit coupling term). Following Refs. 39 and 40 the matrix elements of the interaction potential in the atom–

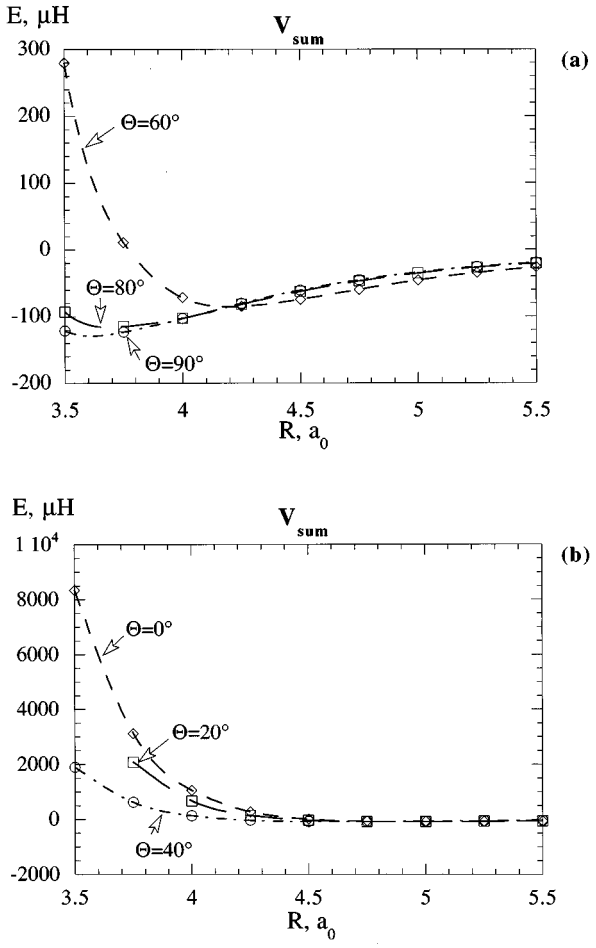

FIG. 9. The R dependence of $V_{\rm sum}=1/2(V_{A'}+V_{A''})$; (a) for $\Theta=90°$, 80°, and 60°; (b) for $\Theta=0°$, 20°, and 40°.

diatom case may be most conveniently represented in terms of the sum and the difference of the A' and A'' potentials

$$V_{\rm sum}=1/2(V_{A'}+V_{A''}),$$

$$V_{\rm diff}=1/2(V_{A'}-V_{A''}).$$

The radial plots of the $V_{\rm sum}$ component at different angles Θ are given in Figs. 9(a) and 9(b). $V_{\rm sum}$ formally retains two minima of the A'' PES, but the collinear minimum is essentially transformed into a wide plateau. The two potentials, $V_{\rm sum}$ and $V_{\rm diff}$, are more relevant to discussing the dynamics in the complex. It should be stressed that in contrast to a closed-shell case, even qualitative predictions are often impossible without actual dynamical calculations which include the spin–orbit coupling effects.

In the present case the spin–orbit splitting of the three $Cl_2(^3\Pi_u)$ states: $^3\Pi_0$, $^3\Pi_1$, and $^3\Pi_2$, is 2–3 orders of magnitude larger than the minute difference of the states A' and A''. Consequently, these three states interacting with He may be approximately described using the $V_{\rm sum}$ potential appropriately modified by spin-orbit coupling, with $V_{\rm diff}$ being negligible. An accurate treatment must solve a set of coupled dynamic equations with an effective Hamiltonian as, e.g., in Ref. 41, and boundary conditions related to either spectroscopy or scattering.

IV. SUMMARY AND CONCLUSIONS

In the present paper we have proposed the decomposition of interaction energy applicable to open shell/excited states systems. This decomposition was used to analyze the origins of the interaction for the $^3A'$ and $^3A''$ states of the $He(^1S)+Cl_2(^3\Pi_u)$ van der Waals complex. In comparison to our previous work,[8] we have presented new, more accurate and complete UMP2 calculations for both states. The $^3A''$ surface possesses two minima, a global one for the T-shaped configuration and a local one for the collinear configuration, which are separated by a low barrier. Only one minimum for the T-shaped structure is present on the $^3A'$ surface. The UMP2 values of D_e and R_e for the T-shaped minimum on the $^3A''$ surface confirm the previously reported[8] data (26.3 cm^{-1} at 3.75 Å). However, the present calculations yield different values for the $^3A'$ state. The D_e for the T-shaped minimum on this surface is deeper by 10 cm^{-1} compared to our previous calculations and now amounts to 27.7 cm^{-1} at 3.75 Å. The best estimates of the global minimum parameters were obtained by using the basis set with bond functions. The UMP2/$spdf(b$-ext) level yields D_e of 31.1 and 28.8 cm^{-1} for the $^3A'$ and $^3A''$ states, respectively. The $A'-A''$ splitting is relatively small and amounts to 2.3 cm^{-1} at the global minimum. The estimates for the linear geometry, where both states converge, are slightly better than those reported before in Ref. 8 and amount to $D_e=18.2$ cm^{-1} and $R_e=5.0$ Å. The improvement was achieved by using the basis set with bond functions. Although UMP2 predicts the $^3A'$ state to be more stable near the T-shaped minimum, the order of the two states reverses at the UMP4 level. Our UMP2/$spdf(b$-ext) binding energies for both states agree well with the experimental value of Benventi *et al.*[6c] who predicted D_e of 32.22 cm^{-1} at 3.56 Å, although the inclusion of higher correlation effects may further increase our D_e values by as much as 3 cm^{-1}.

A small difference between PESs corresponding to the $^3A'$ and $^3A''$ states seems typical for complexes with a π^3 electron occupancy. Such a conclusion was reported by Alexander *et al.*[42] in the case of complexes of Ar with hydrides.[12,43] In our study we find it also true for rare gas atom complexes with halogens. In contrast to π^3, the π^1 electron occupancy [like in Ar–BH($X\,^2\Pi$)[44] or Ar–CH($X\,^2\Pi$)[42]] leads to a large $A'-A''$ splitting. This may be due to the fact that the π^3 configuration always faces a closed shell atom with a π-symmetry orbital (either singly or doubly occupied) but π^1 faces an atom with either π- or σ-symmetry orbitals. A σ orbital reveals a considerably reduced repulsion compared to a π orbital, cf. e.g., CH–He.[45]

We also found that in contrast to the $^3A'$ state, the $^3A''$ state is profoundly similar to the ground state. First, in the region of the middle of the Cl–Cl bond the anisotropies of the $^3A''$ interaction energy, as well as its components, are remarkably close to the ground state, and the resemblance is enhanced upon stretching the Cl–Cl ground state distance. Second, the total PES of $^3A'$ has only one T-shaped minimum, while both $^3A''$ and the ground state have secondary linear minima. The above features may be attributed to the fact that both in the ground state and in the $^3A''$ state the helium atom lies in the plane of the doubly occupied π

orbital, whereas in the $^3A'$ state in the plane of only a singly occupied π orbital.

Interesting aspects of the He–Cl_2 interaction in the $^3A'$ and $^3A''$ states were revealed by analyzing the perturbation components of the interaction energy. First, the global minimum for the T-shaped geometry is related to the niche of the exchange repulsion in the middle of the Cl–Cl bond. The collinear geometry (a minimum only on the A'' PES) corresponds to a maximization of the dispersion attraction.

Second, a comparative analysis of the exchange-repulsion term in the $^3A'$ and $^3A''$ excited states and in the ground state confirms our previous conclusion that the electron cloud is more diffuse in the excited state.[8] Although larger exchange repulsion is accompanied by the increased dispersion attraction, the former seems to be decisive in the minimum and the excited state well depth is smaller. The shape of the electronic density also changes, and in contrast to the ground state it is convex rather than concave at the terminal Cl atoms as was already rationalized in our previous paper.[8] The relative flattening of the ground state density at the Cl end may be attributed to the excess of π contributions (which have nodes on the interatomic axis) over the axially symmetric σ. Indeed, in the excited state one electron is promoted from a π_g orbital to σ_u. Consequently, the excited state has an enhanced σ contribution which favors more charge density at the Cl ends.

The HL-exchange anisotropy indicates that in the middle of the Cl–Cl bond the excited state electron density is also ''thicker'' than in the ground state case (only slightly at the doubly occupied side and more distinctly at the singly occupied side).

Finally, comparison of perturbation components for the $^3A'$ and $^3A''$ states gives new insights into the origin of their difference. The $^3A'$ state is generally lower in energy than the $^3A''$ state, except for geometries involving R shorter than 3.50 Å and Θ near 90°. Qualitatively, this difference is interpreted as a result of the enhanced repulsion in the $^3A''$ state in which the He atom lies in the plane of the doubly occupied π^* orbital of Cl_2. Quantitative details are, however, more difficult to rationalize because the geometries with a stronger exchange repulsion have also stronger induction and dispersion attractions, and vice versa. Yet the general qualitative rule set forth in Ref. 19 stating that the exchange and dispersion determine two different regions of PES, the short- and the long-range, respectively, seems to apply. For the T-shaped form, $^3A'$ has stronger exchange and dispersion and thus it is more repulsive at short range and more attractive at long range. For geometries close to the collinear form of $^3A'$ the situation is less clear.

ACKNOWLEDGMENTS

We thank M. Gutowski for insisting upon using different CP corrections for the A' and A'' states and for many other useful suggestions. We also wish to thank Professor K. C. Janda for valuable discussions. This work was supported by the National Institutes of Health (Grant No. GM36912) and by the Polish Committee for Scientific Research (Grant No. KBN 3T09A 072 09).

[1] R. E. Smalley, D. H. Levy, and L. Wharton, J. Chem. Phys. **64**, 3266 (1976).
[2] D. G. Jahn, S. G. Clement, and K. C. Janda, J. Chem. Phys. **101**, 283 (1994).
[3] S. J. Harris, S. E. Novick, W. Klemperer, and W. E. Falconer, J. Chem. Phys. **61**, 193 (1974).
[4] F.-M. Tao and W. Klemperer, J. Chem. Phys. **97**, 440 (1992).
[5] J. Sadlej, G. Chałasiński, and M. M. Szczęśniak, J. Chem. Phys. **99**, 3700 (1993).
[6] (a) J. I. Cline, D. D. Evard, F. Thommen, and K. C. Janda, J. Chem. Phys. **84**, 1165 (1986); (b) J. I. Cline, B. P. Reid, D. D. Evard, N. Sivakumar, N. Halberstadt, and K. C. Janda, ibid. **89**, 3535 (1988); (c) L. Beneventi, P. Casavecchia, G. G. Volpi, C. R. Bieler, K. C. Janda, *ibid.* **98**, 178 (1993); (d) S. S. Huang, C. R. Bieler, K. C. Janda, F. M. Tao, W. Klemperer, P. Casavecchia, G. G. Volpi, and N. Halberstadt, *ibid.* **102**, 8846 (1995).
[7] D. D. Evard, J. I. Cline, and K. C. Janda, J. Chem. Phys. **88**, 5433 (1988).
[8] G. Chałasiński, M. Gutowski, M. M. Szczęśniak, J. Sadlej, and S. Scheiner, J. Chem. Phys. **101**, 6800 (1994).
[9] J. Sadlej, G. Chałasiński, and M. M. Szczęśniak, Theochem **307**, 187 (1994).
[10] M. H. Alexander, J. Chem. Phys. **99**, 7725 (1993): T. Schmelz, P. Rosmus, and M. H. Alexander, J. Phys. Chem. **98**, 1073 (1994).
[11] R. Jonas and V. Staemmler, Z. Phys. D **14**, 143 (1989).
[12] A. Degli Esposti and H.-J. Werner, J. Chem. Phys. **93**, 3351 (1990).
[13] K. Szalewicz and B. Jeziorski, Mol. Phys. **38**, 191 (1979).
[14] S. Rybak, B. Jeziorski, and K. Szalewicz, J. Chem. Phys. **95**, 6576 (1991).
[15] H. L. Williams, K. Szalewicz, B. Jeziorski, R. Moszynski, and S. Rybak, J. Chem. Phys. **98**, 1279 (1993).
[16] B. Jeziorski, R. Moszyński, and K. Szalewicz, Chem. Rev. **94**, 1887 (1994).
[17] G. Chałasiński and M. M. Szczęśniak, Mol. Phys. **63**, 205 (1988).
[18] S. M. Cybulski, G. Chałasiński, and R. Moszyński, J. Chem. Phys. **92**, 4357 (1990).
[19] G. Chałasiński and M. M. Szczęśniak, Chem. Rev. **94**, 1723 (1994).
[20] (a) P.-O. Löwdin, Adv. Phys. **5**, 1 (1956); (b) B. Jeziorski, M. Bulski, and L. Piela. Int. J. Quantum Chem. **10**, 281 (1976); (c) B. Jeziorski and M. van Hemert, Mol. Phys. **31**, 713 (1976); (d) E. A. Salter, G. W. Trucks, G. Fitzgerald, and R. J. Bartlett, Chem. Phys. Lett. **141**, 61 (1987).
[21] J. H. van Lenthe and F. B. van Duijneveldt, J. Chem. Phys. **81**, 3168 (1984).
[22] B. Bussery and P. E. S. Wormer, J. Chem. Phys. **99**, 1230 (1993).
[23] M. Gutowski, G. Chałasiński, and J. G. C. M. van Duijneveldt-van de Rijdt, Int. J. Quantum Chem. **26**, 971 (1984).
[24] M. Gutowski and L. Piela, Mol. Phys. **64**, 943 (1988).
[25] S. M. Cybulski, J. Chem. Phys. **97**, 7545 (1992).
[26] J. H. van Lenthe, J. G. C. M. van Duijneveldt-van de Rijdt, and F. B. van Duijneveldt, Adv. Chem. Phys. **69**, 521 (1987).
[27] G. Chałasiński and M. Gutowski, Chem. Rev. **88**, 943 (1988).
[28] S. F. Boys and F. Bernardi, Mol. Phys. **19**, 553 (1970).
[29] H.-J. Werner, B. Follmeg, and M. H. Alexander J. Chem. Phys. **89**, 3139 (1988).
[30] GAUSSIAN92, M. J. Frisch, G. W. Trucks, M. Head-Gordon, P. M. W. Gill, M. W. Wong, J. B. Foresman, B. G. Johnson, H. B. Schlegel, M. A. Robb, E. S. Replogle, R. Gomperts, J. L. Andres, K. Raghavachari, J. S. Binkley, C. Gonzalez, R. L. Martin, D. J. Fox, D. J. Defrees, J. Baker, J. J. P. Stewart, and J. A. Pople (Gaussian, Inc., Pittsburgh, 1992).
[31] S. M. Cybulski, TRURL 94 package, Rochester, MI, 1994.
[32] G. Chałasiński, S. M. Cybulski, M. M. Szczęśniak, and S. Scheiner, J. Chem. Phys. **91**, 7048 (1989).
[33] A. J. Sadlej, Coll. Czech. Chem. Commun. **53**, 1995 (1988).
[34] M. Gutowski, F. B. van Duijneveldt, G. Chałasinski, and L. Piela, Mol. Phys. **61**, 233 (1987).
[35] M. Gutowski, J. Verbeek, J. H. van Lenthe, and G. Chałasiński, Chem. Phys. **111**, 271 (1987).
[36] (a) F.-M. Tao and Y.-K. Pan, J. Chem. Phys. **97**, 4989 (1992); (b) F.-M. Tao, *ibid.* **98**, 3049 (1992).
[37] R. Burcl, G. Chałasiński, R. Bukowski, and M. M. Szczęśniak, J. Chem. Phys. **103**, 1498, (1995).
[38] S. Peyerimhoff and R. J. Buenker, Chem. Phys. **57**, 279 (1981).
[39] M. H. Alexander, Chem. Phys. **92**, 337 (1985).
[40] M.-L. Dubernet, D. Flower, and J. M. Hutson J. Chem. Phys. **94**, 7602 (1991).

[41] M.-L. Dubernet and J. M. Hutson, J. Chem. Phys. **99**, 7477 (1993).
[42] M. H. Alexander, S. Gregurick, P. J. Dagdigian, G. W. Lemire, M. J. McQuaid, and R. C. Sausa, J. Chem. Phys. **101**, 4547 (1994).
[43] M. Yang, M. H. Alexander, H.-J. Werner, J. Hohman, L. Neitsch, F. Stuhl, P. J. Dagdigian, J. Chem. Phys. **102**, 4069 (1995).
[44] M. H. Alexander, S. Gregurick, and P. J. Dagdigian, J. Chem. Phys. **101**, 2887 (1994).
[45] S. M. Cybulski, G. Chałasiński, and M. M. Szczęśniak (unpublished).